

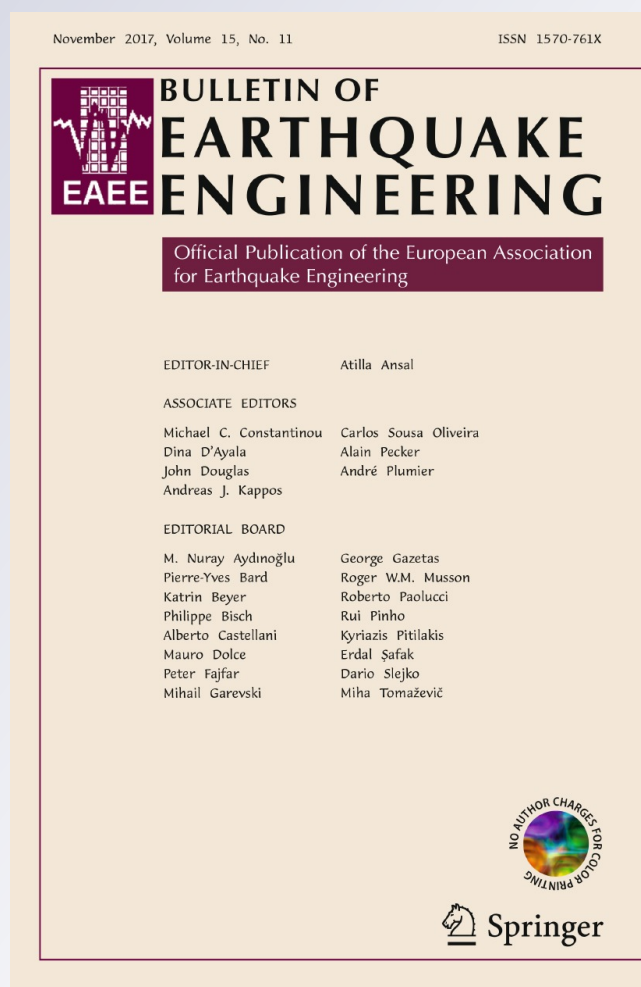
An effective approach for simulating multi-support earthquake underground motions

Guohuan Liu, Jijian Lian, Chao Liang & Mi Zhao

Bulletin of Earthquake Engineering
Official Publication of the European
Association for Earthquake Engineering

ISSN 1570-761X
Volume 15
Number 11

Bull Earthquake Eng (2017)
15:4635-4659
DOI 10.1007/s10518-017-0153-3



Your article is protected by copyright and all rights are held exclusively by Springer Science +Business Media Dordrecht. This e-offprint is for personal use only and shall not be self-archived in electronic repositories. If you wish to self-archive your article, please use the accepted manuscript version for posting on your own website. You may further deposit the accepted manuscript version in any repository, provided it is only made publicly available 12 months after official publication or later and provided acknowledgement is given to the original source of publication and a link is inserted to the published article on Springer's website. The link must be accompanied by the following text: "The final publication is available at link.springer.com".

An effective approach for simulating multi-support earthquake underground motions

Guohuan Liu^{1,2} · Jijian Lian^{1,2} · Chao Liang^{1,2} ·
Mi Zhao³

Received: 16 November 2016 / Accepted: 9 May 2017 / Published online: 17 May 2017
© Springer Science+Business Media Dordrecht 2017

Abstract An effective approach to simulate the multi-support earthquake underground motions is proposed in this paper and the key factor for this approach (i.e. underground cross-correlation function) is presented in advance and elaborated. Previous studies are mainly focused on the multi-support ground motions due to the absence of the necessary conditions to simulate underground motions, i.e., underground power spectral density (PSD), underground response spectrum and, especially, underground cross-correlation function. In this paper, the underground PSD and response spectrum are firstly derived and the cross-correlation function between the underground motions at positions with different horizontal and vertical coordinates is further deduced. The physical meanings of the parameters in this approach are explicitly clarified. Moreover, a program for generating the multi-support earthquake underground motions is developed and the reliability of the generated underground motions is verified. Finally, a two-span bridge is taken as an example to investigate structural responses under multi-support earthquake underground excitations. Numerical results show that the dynamic responses under multi-support earthquake underground motions are significantly different from those under multi-support earthquake ground motions. Results indicate that the simulation of multi-support earthquake underground motions is significant for both study and engineering application.

✉ Guohuan Liu
liugh@tju.edu.cn

✉ Chao Liang
liangchao_0016@sina.cn

¹ State Key Laboratory of Hydraulic Engineering Simulation and Safety, Tianjin University, Tianjin 300072, China

² School of Civil Engineering, Tianjin University, Tianjin 300072, China

³ Key Laboratory of Urban Security and Disaster Engineering of Ministry of Education, Beijing University of Technology, Beijing 100124, China

Keywords Multi-support earthquake underground motions · Underground power spectral density · Underground response spectrum · Underground cross-correlation function · Large-span structure · Seismic response

1 Introduction

Dynamic responses of structures under earthquake excitations are related to and even dependent upon the input method of seismic motion, especially for a large-span structure subjected to multi-support seismic excitations. According to the actual conditions, the earthquake motion is usually characterized by variations in time and space (i.e., the wave passage effect, site coherence effect and local site effect) and the differences in the support motions have a significant influence on the structural internal forces (Hao 1989; Berrah and Kausel 1992). Many theoretical models (especially the coherency function models) are proposed to simulate the spatially varying ground motions. By using the input method of stochastic representations of the seismic ground motions, Zerva (1990) studied the response of continuous multi-span beams of various lengths subjected to spatially varying seismic ground motions. Then, Zerva (2002) further studied the effect of spatial coherency on the seismic response of extended structures from recorded data at dense instrument arrays. Abrahamson et al. (1991) analyzed the spatial coherency of strong ground motion from fifteen earthquakes recorded by the Lotung LSST strong motion array and derived empirical coherency functions for the horizontal component S-waves. Taking different soil conditions into consideration, Kiureghian (1996) proposed a theoretical coherency loss function, in which the ground motion power spectral density function was represented by a site-dependent transfer function and a white noise spectrum and revealed the effect of local site condition on the response of structures across different lengths. Bi and Hao (2011, 2012) firstly investigated the influences of layered irregular sites and random soil properties on coherency functions and then presented an approximate method to simulate spatially varying ground motions on the surface of an uneven site with non-uniform conditions at different locations.

In addition, several investigators have also proposed methods to spatially varying ground motions from different perspectives. Ta et al. (2010) generalized the Soize's model (2006) to account independently for the anisotropy index and the fluctuation level, which leads to major differences in the wave propagation regimes and is beneficial to build the predictive models of the dynamic behavior of inhomogenous and complex structures. Konakli and Der Kiureghian (2012) presented a method for simulating arrays of spatially varying ground motions and validated the correctness of the method by comparing statistical characteristics of the synthetic motions with target theoretical models. Liu et al. (2012) proposed a method for generating multi-point earthquake motions on the basis of focal mechanism. Zentner and Poirion (2012) introduced a new method for generating synthetic ground motion, based on Karhunen–Loève decomposition and a non-Gaussian stochastic model. The proposed method enables the structural analyst to simulate ground motion time histories featuring the properties such as peak ground acceleration (PGA), cumulative absolute velocity and Arias intensity. Su and Shi (2013) proposed a displacement-based earthquake loss assessment methodology for RC frames when the influence of masonry infill panels is taken into account.

Different kinds of structures (e.g., single-span and multi-span bridges, train-bridge system and spatial-reticulated structures, etc.) are taken as examples to investigate structural dynamic responses under multi-support seismic excitations, which are generated by the conventional approach (Lou and Zerva 2005; Alexander 2008; Tian and Yang 2009; Xu 2010; Zhang et al. 2010; Ye et al. 2011; Tian and Li 2012; Guo et al. 2013; Tian et al. 2014; Shrestha et al. 2014). A new methodology is set up and implemented into a computer code by Sextos et al. (2003) for deriving sets of appropriately modified time histories and spring–dashpot coefficients at each support of a bridge with account for spatial variability, local site conditions and soil–foundation–superstructure interaction, for the purposes of inelastic dynamic analysis of RC bridges. Several investigators (Berrah and Kausel 1992; Kiureghian and Neumhofer 1992; Su et al. 2006; Yu and Zhou 2008) extended the response spectrum method for the case of spatially varying ground excitations to estimate the peak structural response. However, above studies are mainly focused on earthquake ground motions and the multi-support earthquake underground motions are rarely reported in the published literatures. It is noted that for the large-span spatial structure with underground structure, regarding ground motions as underground input is unreasonable. According to Zerva's productive work (2009), the seismic ground deformations are selected as the seismic loads for the underground structures (e.g. buried pipelines and tunnels). However, there continues to be a lack of effective theoretical approaches to simulate the multi-support underground earthquake motions (e.g. acceleration, velocity and displacement time histories).

For the seismic analysis of spatial system with underground structure, one may input the multi-point earthquake excitations at the base of the building. In this case, the underground excitation is generated by the seismic wave propagating to the base of the underground structure at a certain depth below the ground. The existing ground PSD, response spectrum and coherence models cannot be directly employed to simulate the multi-support underground motions. Therefore, the underground PSD and underground response spectrum are firstly deduced and then the underground cross-correlation function is further presented. These three theoretical models are firstly employed to establish the total power spectrum matrix and then the underground motions are generated by decomposing the aforementioned matrix using Cholesky decomposition method. These three theoretical models are not only necessary conditions to simulate the multi-support earthquake underground motions but also the standards to verify the simulation results. Moreover, a program for simulating multi-support earthquake underground motions is developed and its reliability is verified. Finally, a two-span bridge is taken as an example to calculate its seismic response under both multi-support earthquake ground and underground motions. Numerical results show that the simulation of multi-support earthquake underground motions is significant for both study and engineering application.

2 Review of transfer function

2.1 Transfer function for simple layer soil

Figure 1 gives one-dimensional system consists of two horizontal layers which extends to infinity in the horizontal direction and has a half-space as the bottom layer. The parameters z and h are the ordinate values of layer and the soil layer height, respectively; A and B are

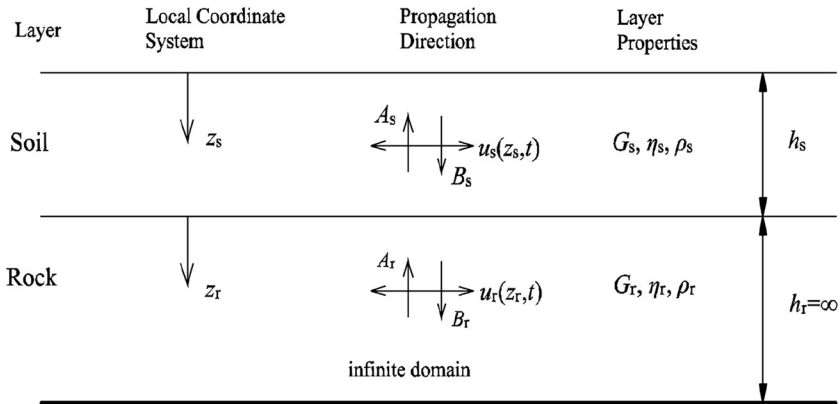


Fig. 1 The propagation of shear wave in simple layer soil

the amplitudes of the up-going and down-going waves, respectively; the subscripts s and r relate to the value of the associated variable in soil and rock layer, respectively; $u(z, t)$ denotes the horizontal displacement function; ρ , G , and η are soil/rock density, shear modulus and viscous coefficient.

The equation for a one-dimensional wave can be expressed as follows

$$\rho \frac{\partial^2 u_s}{\partial t^2} = G \frac{\partial^2 u_s}{\partial z_s^2} + \eta \frac{\partial^3 u_s}{\partial z_s^2 \partial t} \tag{1}$$

The displacement function with circular frequency ω is determined as (Schnabel et al. 1972)

$$u_s(z_s, t) = U(z_s)e^{i\omega t} \tag{2}$$

Substituting Eq. (2) into Eq. (1) and solving the obtained equation yields

$$U(z_s) = Ae^{ik_s^* z_s} + Be^{-ik_s^* z_s} \tag{3}$$

where k_s^* and G^* are complex wave number and complex shear modulus, respectively and satisfy the following relationship (Schnabel et al. 1972)

$$(k_s^*)^2 = \frac{\rho\omega^2}{G + i\omega\eta} = \frac{\rho\omega^2}{G^*} \tag{4a}$$

$$G^* = G + i\omega\eta \tag{4b}$$

$$\omega\eta = 2G\xi \tag{4c}$$

Substituting Eq. (4c) into Eq. (4b) yields

$$G^* = G(1 + 2i\xi) \tag{4d}$$

where G^* can be assumed to be independent of frequency.

Combining Eq. (2) and Eq. (3) yield the following displacement functions

$$u_s(z_s, t) = A_s e^{i(\omega t + k_s^* z_s)} + B_s e^{i(\omega t - k_s^* z_s)} \tag{5}$$

$$u_r(z_r, t) = A_r e^{i(\omega t + k_r^* z_r)} + B_r e^{i(\omega t - k_r^* z_r)} \tag{6}$$

Considering the boundary conditions at the bedrock-soil interface ($u_s = u_r, \tau_s = \tau_r$) and the free surface of ground ($\tau_s = 0$), the following equations yield

$$A_s (e^{ik_s^* h} + e^{-ik_s^* h}) = A_r + B_r \tag{7}$$

$$\alpha_z^* A_s (e^{ik_s^* h} - e^{-ik_s^* h}) = A_r - B_r \tag{8}$$

where

$$\alpha_z^* = \frac{G_s^* k_s^*}{G_r^* k_r^*} \tag{9}$$

is referred to as a complex impedance ratio.

Solving Eqs. (7) and (8) and employing Euler’s Law (SHAKE2000 Consulting Group User’s Manual 2000), the transfer function between soil and rock can be obtained

$$H_{sr}(\omega) = \frac{1}{\cos k_s^* h + i \alpha_z^* \sin k_s^* h} \tag{10}$$

2.2 The change of phase angle

Obviously, for the term $B_s e^{i(\omega t - k_s^* z_s)}$ in Eq. (5), the imaginary parts cancel each other out while the real parts are combined with each other. The displacement function is given by (Schnabel et al. 1972; SHAKE2000 Consulting Group User’s Manual 2000)

$$u_s(z_s, t) = 2A_s \cos(\omega t + k_s^* z_s) \tag{11}$$

The amplitude, period and phase angle of $u_s(z_s, t)$ are illustrated in Fig. 2 and the phase angle can be expressed as the following equation

$$\tau = \frac{k_s^* z_s}{\omega} = \sqrt{\frac{\rho}{G^*}} z_s \tag{12}$$

The phase angle τ varies with the ordinate value z_s .

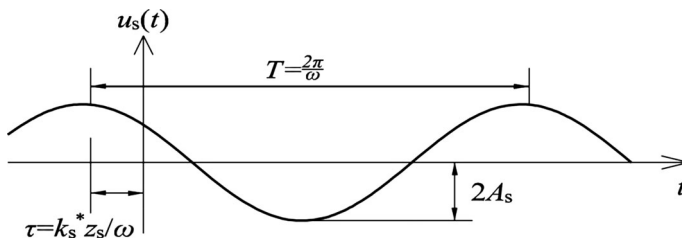


Fig. 2 The amplitude, period and phase angle of $u_s(z_s, t)$

2.3 Transfer function for multi-layer soil

As shown in Fig. 3, z denotes the ordinate value of layer and in addition the coordinate origins are located at the top of each layer; h denotes the layer height; A and B are the amplitudes of the up-going and down-going waves, respectively; the subscript n is the sequence number of soil layer; $H_{ij}(\omega)$ denotes the transfer function.

Wave propagations in multi-layered and simple layer soil, as shown in Figs. 1 and 3, are similar, and the transfer function for multi-layer condition is more complex than that for simple layer condition. Based on the above analysis, the horizontal displacement formula for the j th layer is

$$u_j(z_j, t) = A_j e^{i(\omega t + k_j^* z_j)} + B_j e^{i(\omega t - k_j^* z_j)} \tag{13}$$

According to the displacement coordination and the shear stress continuity at the interface between j th and $(j + 1)$ -th soil layer, the following equations must be satisfied

$$A_j e^{ik_j^* h_j} + B_j e^{-ik_j^* h_j} = A_{j+1} + B_{j+1} \tag{14}$$

$$\alpha_j^* (A_j e^{ik_j^* h_j} - B_j e^{-ik_j^* h_j}) = A_{j+1} - B_{j+1} \tag{15}$$

where α_j^* is the complex impedance ratio and defined as

$$\alpha_j^* = \frac{G_j^* k_j^*}{G_{j+1}^* k_{j+1}^*} \tag{16}$$

Combining Eqs. (14) and (15) yield

$$A_{j+1} = \frac{1}{2} A_j \left[(1 + \alpha_j^*) e^{ik_j^* h_j} + (1 - \alpha_j^*) e^{-ik_j^* h_j} \right] \tag{17a}$$

$$B_{j+1} = \frac{1}{2} A_j \left[(1 - \alpha_j^*) e^{ik_j^* h_j} + (1 + \alpha_j^*) e^{-ik_j^* h_j} \right] \tag{17b}$$

Considering that there is no shear stress at the ground surface, the displacement of $(j + 1)$ -th layer can be obtained from the following formulae

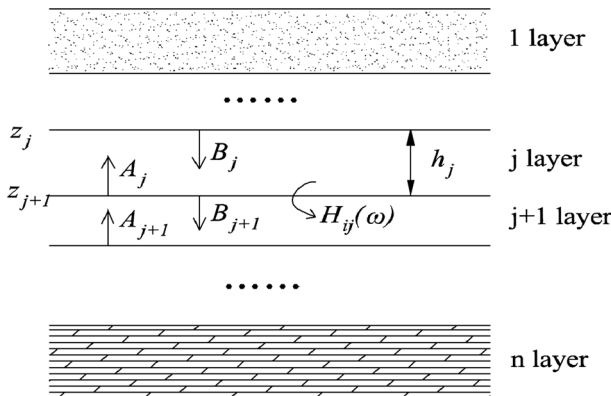


Fig. 3 Wave propagation in multi-layer soil

$$A_{j+1} = a_{j+1}^*(\omega)A_1 \tag{18a}$$

$$B_{j+1} = b_{j+1}^*(\omega)B_1 \tag{18b}$$

$$A_1 = B_1 \tag{19}$$

where $a_{j+1}^*(\omega)$ and $b_{j+1}^*(\omega)$ are the recursive coefficients derived from Eq. (17a) and (17b), respectively.

The transfer function between any two layers can be calculated from the following equation

$$H_{ij}(\omega) = \frac{a_i^*(\omega) + b_i^*(\omega)}{a_j^*(\omega) + b_j^*(\omega)} \tag{20}$$

3 Underground PSD and response spectrum

To provide an effective approach to simulate the corresponding multi-support seismic underground motions, the former two necessary conditions to simulate underground motions (i.e., underground power spectral density (PSD) and underground response spectrum) are given on the basis of those conditions of ground motions random vibration theory, and the detailed derivation process is given in this section. Another necessary condition (i.e., underground coherence function) for simulating multi-support seismic underground motions is given in Sect. 4.

The geological strata geometry is given in Fig. 4.

The relationship among $S_{mm}(\omega)$, $S_{ii}(\omega)$ and $H_{im}(\omega)$ is

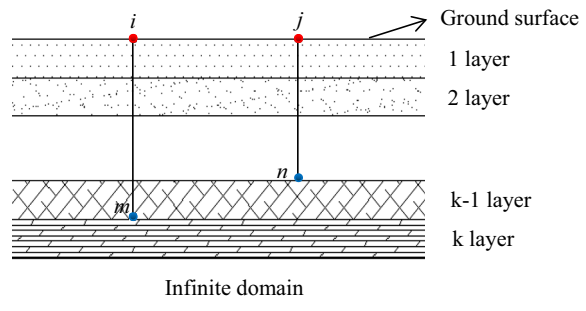
$$\frac{S_{mm}(\omega)}{S_{ii}(\omega)} = |H_{im}(\omega)|^2 \tag{21}$$

where $S_{ii}(\omega)$ and $S_{mm}(\omega)$ are the auto-power spectrum of the motions at points i and m , respectively.

Most of the formulae about the response spectrum can be written in the following form (Clough and Penzien 1993; Chopra 2001)

$$R_i(\omega, \zeta) \approx k_i \sqrt{S_{ii}(\omega)} \tag{22}$$

Fig. 4 Geological strata geometry



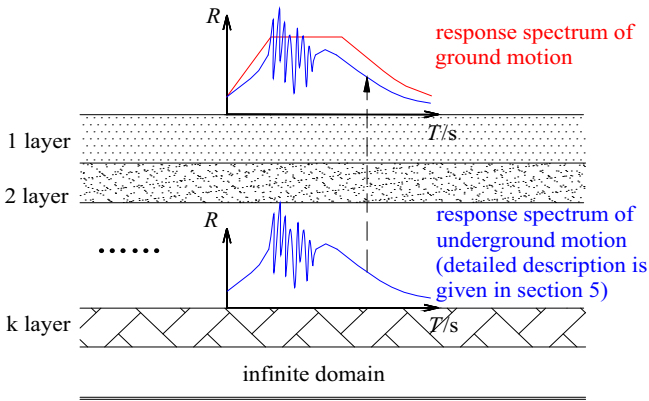


Fig. 5 Response spectrum for ground and underground motions. R is the earthquake influence coefficient (the ratio of the spectral acceleration to the maximum acceleration); T is the natural period of structure

where k_i denotes peak factor related to exceeding probability, period, circular frequency and damping ratio; $S_{ii}(\omega)$ is the auto-PSD. In the general case, parameter k is given by (Clough and Penzien 1993; Chopra 2001)

$$k = \sqrt{-2 \ln \left(-\frac{\pi \ln p}{\omega \bar{T}} \right)} \left(\frac{\pi \omega}{2\xi} \right)^{1/2} \tag{23}$$

where \bar{T} denotes the duration of the signal, p denotes the non-exceedance probability value. The relationship between $R_m(\omega, \xi)$ and $R_i(\omega, \xi)$ is

$$\frac{R_m(\omega, \xi)}{R_i(\omega, \xi)} = \frac{k_m}{k_i} \sqrt{\frac{S_{mm}(\omega)}{S_{ii}(\omega)}} \tag{24}$$

Substituting Eq. (23) into Eq. (24) yields

$$\frac{R_m(\omega, \xi)}{R_i(\omega, \xi)} = \frac{\sqrt{-2 \ln \left(-\frac{\pi \ln p}{\omega \bar{T}} \right)} \left(\frac{\pi \omega}{2\xi} \right)^{1/2}}{\sqrt{-2 \ln \left(-\frac{\pi \ln p}{\omega \bar{T}} \right)} \left(\frac{\pi \omega}{2\xi} \right)^{1/2}} \sqrt{\frac{S_{mm}(\omega)}{S_{ii}(\omega)}} = |H_{im}(\omega)| \tag{25}$$

Figure 5 is given for the comparison between the ground and underground response spectrums. In addition, the detailed description of response spectrum of underground motion is given in Sect. 4.

4 Derivation of underground coherence function for multi-support earthquake motions

As shown in Fig. 6, the relationship of phase differences between harmonic motions is given. The terms $i^{(\omega)}(t)$ and $i^{(\omega)}(t + \tau_i)$ are the harmonic motions with phase difference τ_i ; $j^{(\omega)}(t + \Delta\tau_1)$ and $j^{(\omega)}(t + \Delta\tau_1 + \tau_j)$ are the harmonic motions with phase difference τ_j ; $\Delta\tau_1$

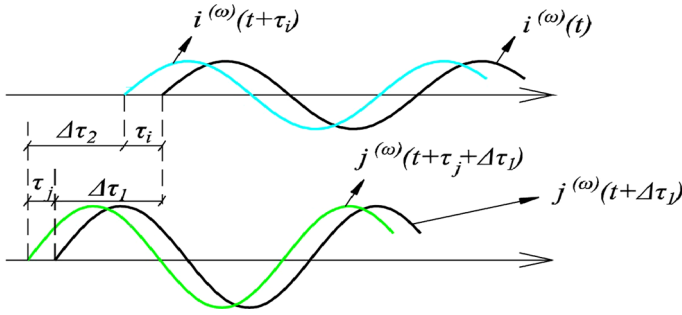


Fig. 6 Harmonic motions with different phase differences

is the phase difference between $i^{(\omega)}(t)$ and $j^{(\omega)}(t + \Delta\tau_1)$; $\Delta\tau_2$ is the phase difference between $i^{(\omega)}(t + \tau_i)$ and $j^{(\omega)}(t + \Delta\tau_1 + \tau_j)$.

The expression of the cross-PSD is given by

$$S_{ij}(\omega) = \frac{1}{2\pi} \int_{-\infty}^{\infty} R_{ij}(\Delta\tau_1) e^{-i\omega\Delta\tau_1} d\Delta\tau_1 \tag{26}$$

where $R_{ij}(\Delta\tau_1)$ is the cross correlation function between the motions at points i and j , defined as

$$R_{ij}(\Delta\tau_1) = E \left[i^{(\omega)}(t) j^{(\omega)}(t + \Delta\tau_1) \right] \tag{27}$$

From Fig. 6, the vibration of point j can be expressed by that of point i with a phase difference

$$j^{(\omega)}(t + \Delta\tau_1) = \frac{A^{(j)}}{A^{(i)}} i^{(\omega)}(t + \tau_i - \tau_j + \Delta\tau_2) \tag{28}$$

where A represents the amplitude of harmonic vibration; superscripts i and j relate to the value of the associated variable of harmonic motions at points i and j , respectively.

Substituting Eq. (28) into Eq. (27) yields

$$R_{ij}(\Delta\tau_1) = E \left[i^{(\omega)}(t) \frac{A^{(j)}}{A^{(i)}} i^{(\omega)}(t + \tau_i - \tau_j + \Delta\tau_2) \right] = \frac{A^{(j)}}{A^{(i)}} R_{ii}(\tau_i - \tau_j + \Delta\tau_2) \tag{29}$$

Substituting Eq. (29) into Eq. (26) gives

$$\begin{aligned} S_{ij}(\omega) &= \frac{A^{(j)}}{2\pi A^{(i)}} \int_{-\infty}^{\infty} R_{ii}(\tau_i - \tau_j + \Delta\tau_2) e^{-i\omega\Delta\tau_1} d\Delta\tau_1 \\ &= \frac{A^{(j)}}{2\pi A^{(i)}} \int_{-\infty}^{\infty} R_{ii}(\tau_i - \tau_j + \Delta\tau_2) e^{-i\omega\Delta\tau_2} e^{i\omega(\tau_j - \tau_i)} d(\tau_i - \tau_j + \Delta\tau_2) \end{aligned} \tag{30}$$

where τ_i and τ_j are constants; $\Delta\tau_2$ is the integral variable.

It is important to note that the initial phase difference has no effect on the final results, when the integral interval tends to infinity. Therefore, Eq. (26) can be further rewritten as

$$\begin{aligned}
 S_{ij}(\omega) &= \frac{A_{(\omega)}^{(j)}}{2\pi A_{(\omega)}^{(i)}} \int_{-\infty}^{\infty} R_{ii}(\Delta\tau_2) e^{-i\omega\Delta\tau_2} e^{i\omega(\tau_j-\tau_i)} d(\Delta\tau_2) \\
 &= \frac{A_{(\omega)}^{(j)}}{2\pi A_{(\omega)}^{(i)}} e^{i\omega(\tau_j-\tau_i)} S_{ii}(\omega)
 \end{aligned}
 \tag{31}$$

The cross-PSD for the underground motions, $S_{mn}(\omega)$, can be similarly expressed as

$$S_{mn}(\omega) = \frac{A_{(\omega)}^{(n)}}{2\pi A_{(\omega)}^{(m)}} e^{i\omega(\tau_n-\tau_m)} S_{mm}(\omega)
 \tag{32}$$

Therefore, the relationship between $S_{ij}(\omega)$ and $S_{mn}(\omega)$ is

$$\begin{aligned}
 \frac{S_{mn}(\omega)}{S_{ij}(\omega)} &= \frac{\frac{A_{(\omega)}^{(n)}}{2\pi A_{(\omega)}^{(m)}} e^{i\omega(\tau_n-\tau_m)} S_{mm}(\omega)}{\frac{A_{(\omega)}^{(j)}}{2\pi A_{(\omega)}^{(i)}} e^{i\omega(\tau_j-\tau_i)} S_{ii}(\omega)} \\
 &= e^{i\omega(\tau_i-\tau_m)} e^{i\omega(\tau_n-\tau_j)} |H_{im}(\omega)| |H_{jn}(\omega)|
 \end{aligned}
 \tag{33}$$

The two coherence functions for earthquake ground and underground motions, $\rho_{ij}(\omega)$ and $\rho_{mn}(\omega)$, are given by the following formulae

$$\rho_{ij}(\omega) = \frac{S_{ij}(\omega)}{\sqrt{S_{ii}(\omega)S_{jj}(\omega)}}
 \tag{34}$$

$$\rho_{mn}(\omega) = \frac{S_{mn}(\omega)}{\sqrt{S_{mm}(\omega)S_{nn}(\omega)}}
 \tag{35}$$

Combining Eqs. (34) and (35) yields

$$\frac{\rho_{mn}(\omega)}{\rho_{ij}(\omega)} = \frac{S_{mn}(\omega)}{S_{ij}(\omega)} \frac{\sqrt{S_{ii}(\omega)S_{jj}(\omega)}}{\sqrt{S_{mm}(\omega)S_{nn}(\omega)}} = \frac{S_{mn}(\omega)}{S_{ij}(\omega)} |H_{mi}(\omega)| |H_{nj}(\omega)|
 \tag{36}$$

Then, $\frac{\rho_{mn}(\omega)}{\rho_{ij}(\omega)}$ can be calculated from Eqs. (33) and (36)

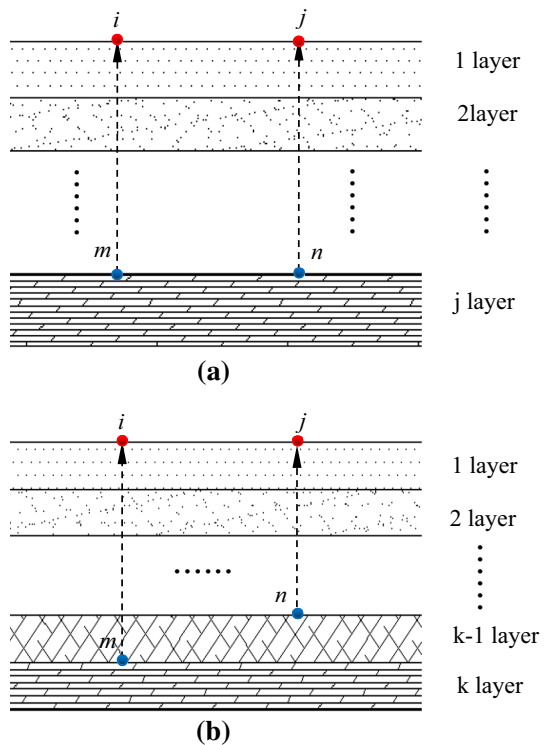
$$\frac{\rho_{mn}(\omega)}{\rho_{ij}(\omega)} = e^{i\omega(\tau_i-\tau_m)} e^{i\omega(\tau_n-\tau_j)} = e^{i\omega[(\tau_i-\tau_m)-(\tau_j-\tau_n)]}
 \tag{37}$$

The value of τ_i, τ_j, τ_m and τ_n can be calculated by Eq. (12) given in Sect. 2.2.

$$\tau = \frac{k^*z}{\omega} = \sqrt{\frac{\rho}{G^*}}z$$

The density ρ and the complex shear modulus G^* are determined by certain layers. Therefore, the phase difference between the ground and underground sinusoidal waves is dominated by z_s of each layer. In the case that the thickness of the same soil layer is

Fig. 7 Geological strata geometries in different cases. **a** Geological strata geometry for $\rho_{mn}(\omega) = \rho_{ij}(\omega)$, **b** Geological strata geometry for $\rho_{mn}(\omega) \neq \rho_{ij}(\omega)$



uniform, as shown in Fig. 7a, $(\tau_i - \tau_m)$ is equal to $(\tau_j - \tau_n)$ and $\rho_{mn}(\omega)/\rho_{ij}(\omega)$ turns out to be 1. However, in general conditions, the thickness of the same soil layer is not uniform (Fig. 7b), and then $(\tau_i - \tau_m)$ is not equal to $(\tau_j - \tau_n)$ because z_s varies with the location even in the same layer. Therefore, the ratio of $\rho_{mn}(\omega)/\rho_{ij}(\omega)$ is not equal to 1.0.

According to the above analysis, all of the necessary conditions to simulate underground motions (i.e., underground power spectral density (PSD), underground response spectrum and underground cross-correlation function) are derived on the basis of those necessary conditions of ground motion. Based on the proposed approach, the coherency model for the underground motion is theoretically compatible with that for the free surface ground motion. In engineering practice, the precise knowledge of the subsoil configuration is difficult to obtain. If the precise subsoil configuration is obtained using current geological exploration technology, the underground seismic motion can be simulated for the far-fault earthquake based on the proposed approach.

5 Program development and verification for multi-support earthquake underground motions

5.1 Flowchart of program development

Based on the above analysis, a flowchart including nine steps for computing the PSD, response spectrum and coherence function of the underground motions is given in Fig. 8.

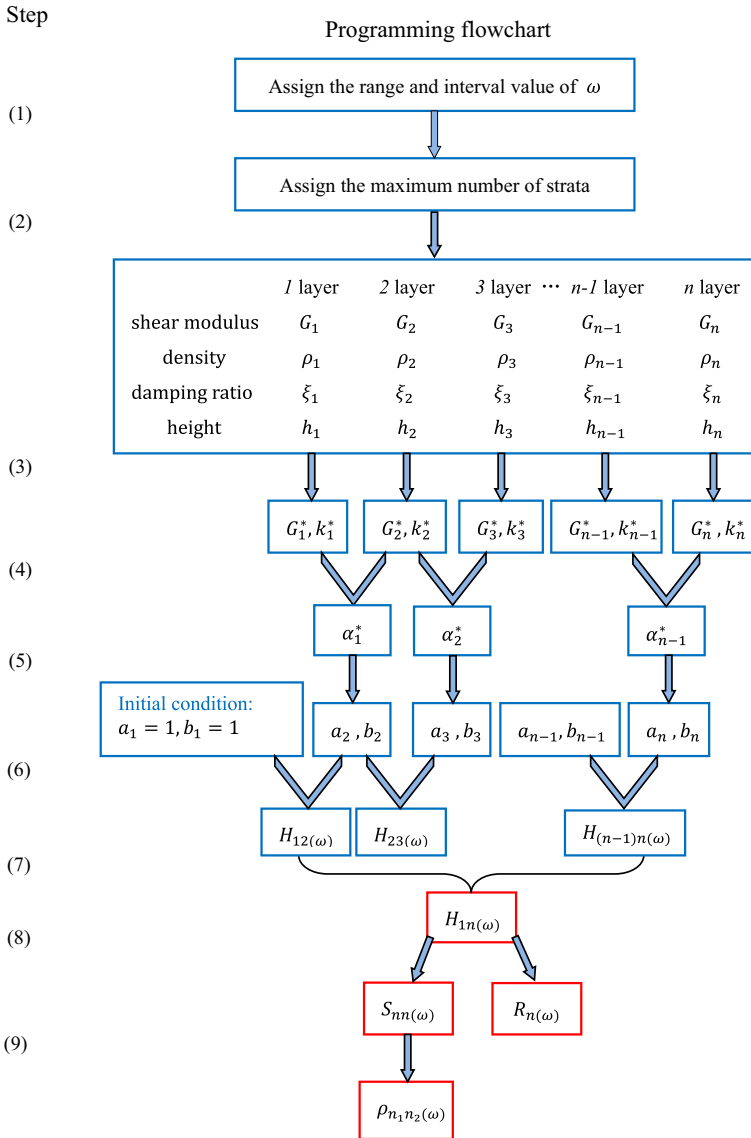


Fig. 8 Programming flowchart for calculating the PSD, response spectrum and coherence function of the underground motions

5.2 Development and verification of program

In order to verify the reliability of the developed program, an analysis based on the geological parameters listed in Table 1 is performed. As shown in Fig. 9, the points A', B' and C' are located in different soil layers, the thicknesses of the soil between ground surface and points A', B' and C' are different from each other. Therefore, three sets of thickness data are assigned and the transfer functions are calculated based on these

Table 1 Material parameters of layered soil

Layer	Density (kg/m ³)	Elastic modulus (MPa)	Poisson's ratio	Damping ratio	Thickness (m)		
1	1830	430	0.26	0.05	30	30	30
2	1870	490	0.29	0.05	30	30	30
3	1920	550	0.32	0.05	30	30	30
4	1970	610	0.35	0.05	30	30	30

* E represents the elastic modulus; ν represents the Poisson's ratio. Shear modulus is denoted as $G = E/2(1 + \nu)$

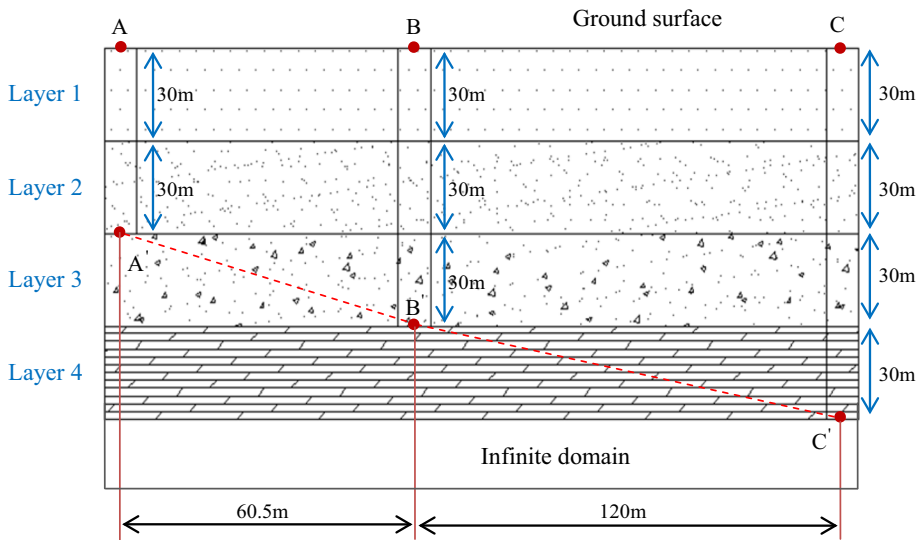


Fig. 9 Comparison of the positions at different depths

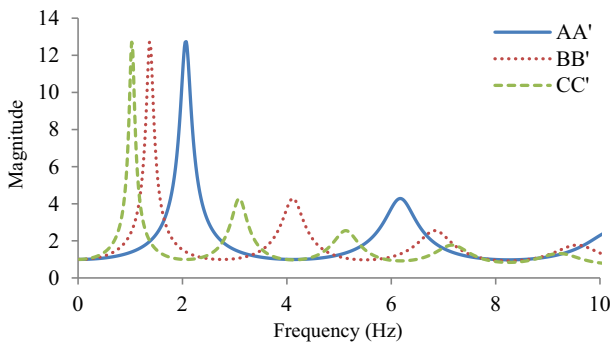


Fig. 10 Transfer functions of different positions at different depths

parameters and the above theoretical analysis. Figure 10 indicates that the dominant frequency of transfer function decreases with increasing thickness, which is consistent with the actual phenomenon.

In order to generate the earthquake underground motions, the relevant parameters should be assigned in advance. The PSD model, coordinates of support points, apparent wave velocity, coherence function, response spectrum and intensity envelope function are assigned after the transfer function is obtained for calculating the underground motions.

Clough–Penzien model is adopted as the ground target PSD

$$S(\omega) = \frac{\omega_g^4 + 4\zeta_g^2\omega_g^2\omega^2}{(\omega_g^2 - \omega^2)^2} \cdot \frac{\omega^4}{(\omega_f^2 - \omega^2)^2 + 4\zeta_f^2\omega_f^2\omega^2} S_0 \tag{38}$$

where S_0 is the spectral intensity; ω is circular frequency; ω_g and ζ_g are the ground predominant frequency and ground damping ratio, respectively; ω_f and ζ_f are seismic energy parameters which reflect the changes of seismic energy of low frequency. In this paper, the values of S_0 , ω_g , ζ_g , ω_f , and ζ_f (Maharaj 1978; Liu et al. 2009) are assigned to 0.042, 21.40, 0.075, 0.38, and 0.49, respectively.

Hao coherent model (Liu et al. 2009; Hao et al. 1989) is adopted as ground target coherence function

$$\rho_{jk}(\omega, d) = e^{(-\beta_1 d)} \cdot e^{[-a_1(\omega)\sqrt{d}(\frac{\omega}{\beta_1})^2]} \tag{39}$$

$$a_1(\omega) = \frac{2\pi a}{\omega} + \frac{b\omega}{2\pi} + c \tag{40}$$

where ρ_{jk} is the coherence function between the motions of support points j and k ; ω is circular frequency; the time lag $\tau = d/v_{app}$ with v_{app} denotes the surface apparent wave velocity and d is the distance between j and k ; β_1 , a , b and c are constants, and are assigned to 1.109×10^{-4} , 3.583×10^{-2} , -1.811×10^{-5} and -1.177×10^{-4} (Maharaj 1978; Liu et al. 2009), respectively.

The PSD function is first obtained on the basis of Clough–Penzien model and Hao coherent model, and the cross-PSD function is also obtained accordingly. The PSD matrix can be represented by the PSD function and cross-PSD function based on stationary random theory (Zerva 2002). Moreover, the PSD matrix is decomposed by Cholesky Decomposition Method (Atkinson 1978) to calculate the amplitude and the phase angle. Then, the ground motions are generated through prototype spectral representation method (Hao et al. 1989). According to Eqs. (21) and (37), the underground PSD and coherence function can be calculated directly and the underground motions can be simulated in the same way. In this paper, the apparent wave velocity is 250 m/s, and the parameters of intensity envelope function, i.e., t_1 , t_2 and c are set to 0.8, 7.0 and 0.35, respectively. Response spectrum of Bridge Seismic Design Code (MOHURD 2011) is adopted as the ground target response spectrum. Eventually, the acceleration histories, peak values and variances of the earthquake underground motions are simulated and illustrated in Fig. 11.

As shown in Fig. 11, the peak values and variances of underground motions are smaller than those of ground motions, which indicates that the earthquake motions are amplified by layered soil deposits. Figures 12 and 13 show that the simulated PSD of ground and underground motions are coherent with the target PSD. In addition, it should be emphasized that the curves of underground target PSD are undulate and exhibit a significant difference from the smooth curves of the ground target PSD. From Eq. (21) and Fig. 14,

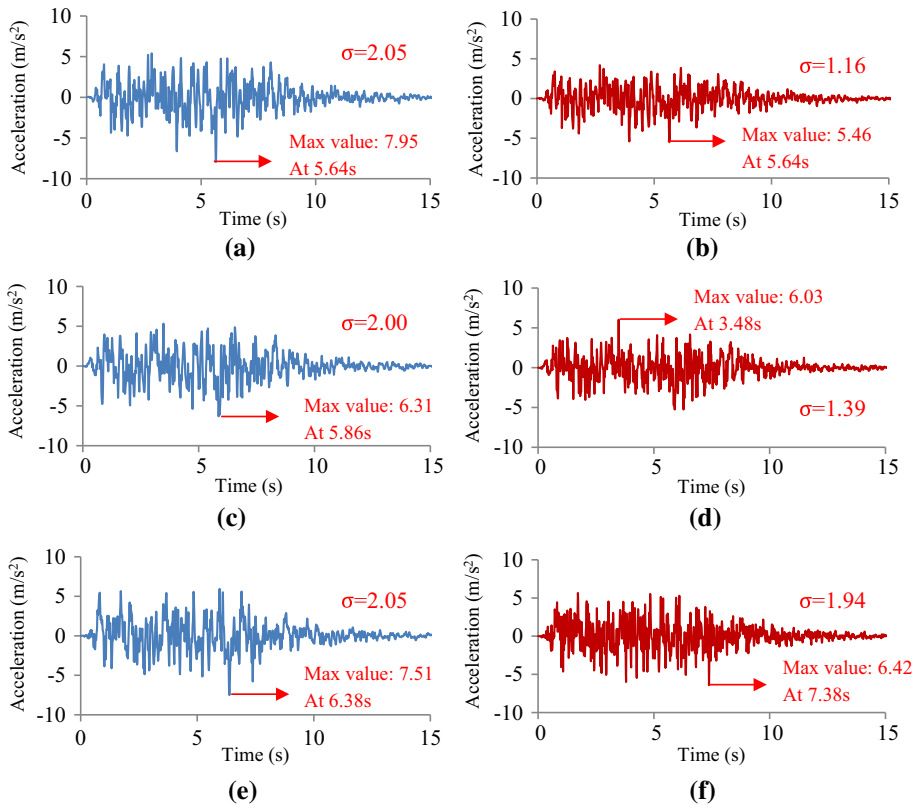


Fig. 11 The ground and underground acceleration histories. σ is the variance of the acceleration history. **a** Location A, **b** Location A', **c** Location B, **d** Location B', **e** Location C, **f** Location C'

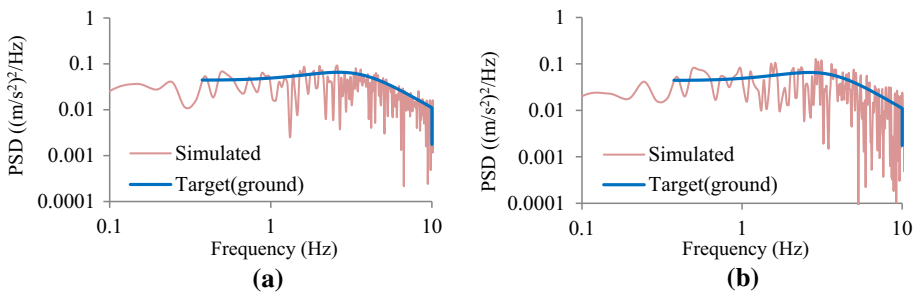


Fig. 12 Comparison between target and simulated PSD of ground motions. Double logarithmic coordinate. **a** Location A, **b** Location B

the essential reason for the phenomenon is that $S_{mm}(\omega)$ is the product of $S_{ii}(\omega)$ (smooth and characterized by statistical properties) and $|H_{im}(\omega)|^2$ which is unstatistical, undulate and dependent on the specific soil properties.

According to Fig. 15, coherence coefficients of both ground and underground target coherence functions approach to 1 when the frequency approaches to 0. Moreover, the

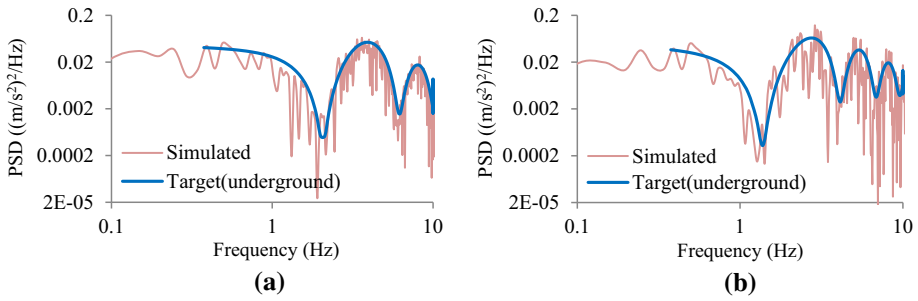


Fig. 13 Comparison between target and simulated PSD of underground motions. Double logarithmic coordinate. **a** Location A', **b** Location B'

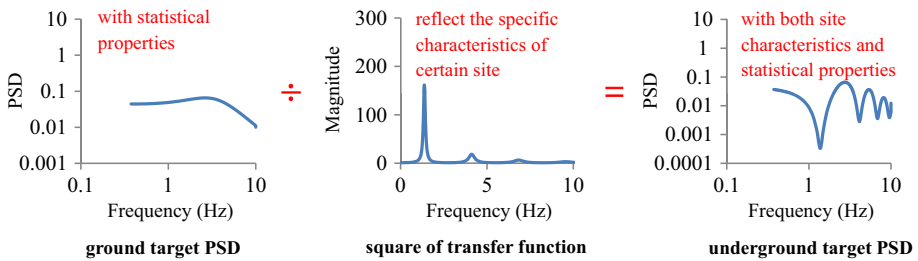


Fig. 14 Generation of underground target PSD

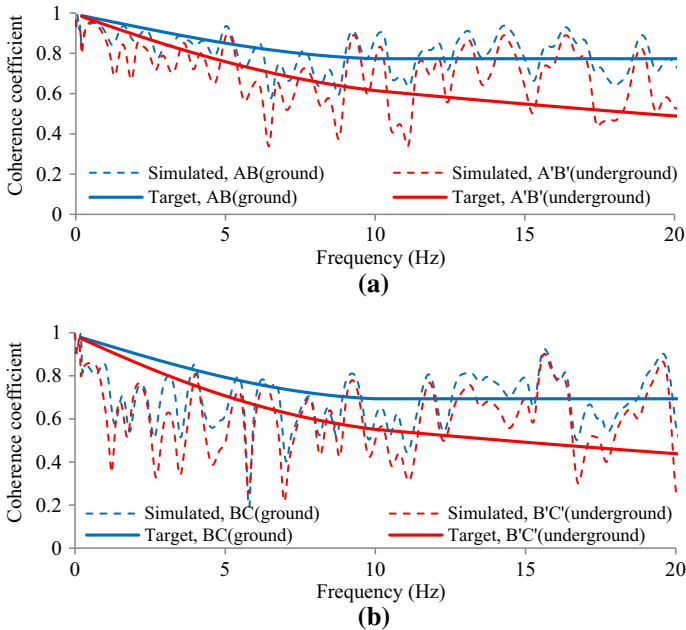


Fig. 15 Comparison between target and simulated coherence functions. **a** Location AB (A'B'), **b** Location BC (B'C')

difference between the ground and underground target coherence functions becomes more significant with increasing frequency. The reason is that in Eq. (39), the first exponent, $-\beta_1 d$, is a very small constant and the second exponent, $-a_1(\omega)\sqrt{d}(\omega/2\pi)^2$, approaches to 0 with decreasing frequency. Hence, the values of both ground and underground coherent coefficients approach to 1 when the frequency approaches to 0. According to Eq. (37), $\rho_{im}(\omega)/\rho_{ij}(\omega)$ decreases from 1 to infinitesimal with the increase of circular frequency. Therefore, the differences between coherence coefficients in the high-frequency domain are more significant than that in the low-frequency domain. The coherence coefficient of each frequency shown in Fig. 15b is a little smaller than that shown in Fig. 15a because the distance between A(A') and B(B') is smaller than the distance between B(B') and C(C').

The response spectrum of bridge seismic design code (MOHURD 2011) shown in Fig. 16 is adopted as the target response spectrum. It is noted that the underground target response spectrum fluctuates violently because the underground target response spectrum is calculated from

$$\frac{R_m(\omega, \xi)}{R_i(\omega, \xi)} = |H_{im}(\omega)| \tag{41}$$

in which $|H_{im}(\omega)|$ is undulate while $R_i(\omega, \xi)$ is smooth. Figure 17 is given to explain it more clearly. It can be seen from Fig. 16 that the period corresponding to the platform stage of the ground target response spectrum ranges from 0.101 to 0.347 s. The average value of the underground target response spectrum over the period range from 0.101 to 0.347 s is highlighted. This average value is smaller than the value of the platform stage of ground target response spectrum, which reflects the aforementioned site amplification

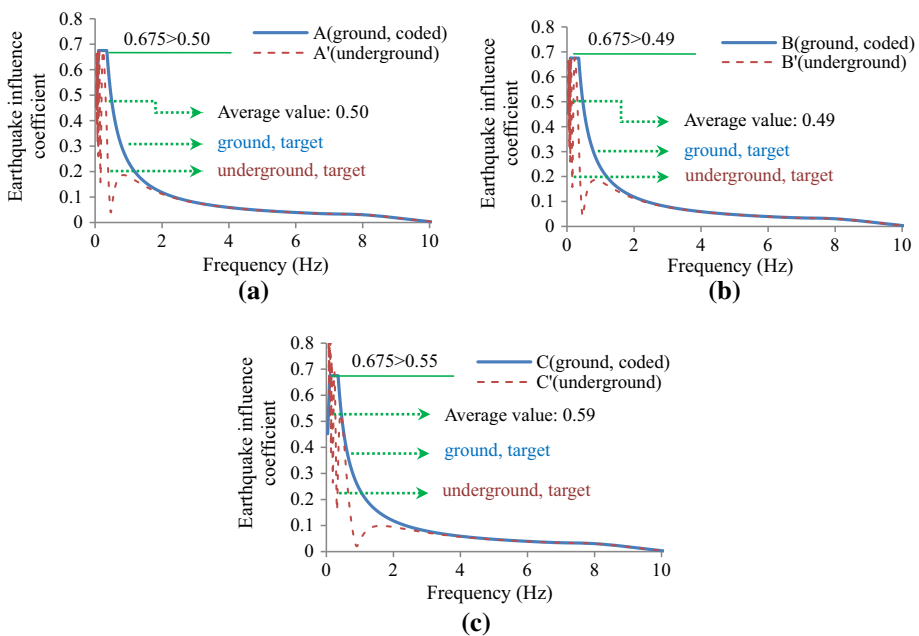


Fig. 16 Comparison between target response spectrums of ground and underground motions. **a** Location AA', **b** Location BB', **c** Location CC'

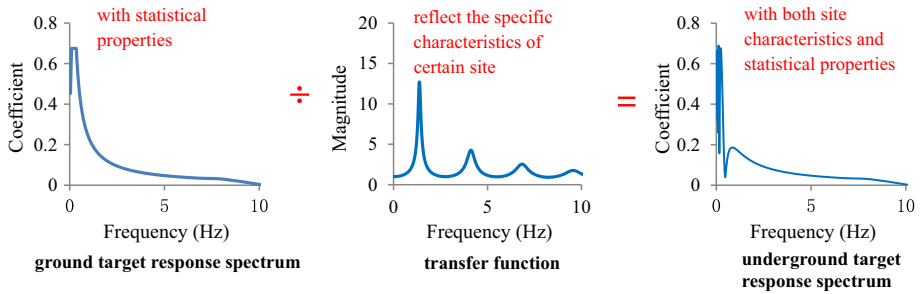


Fig. 17 Generation of underground target response spectrum

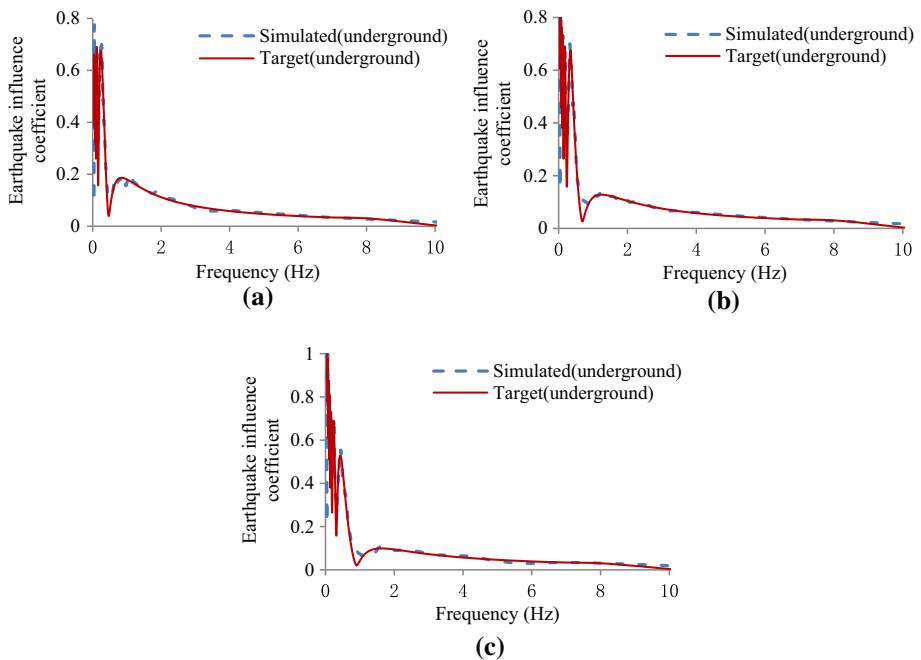


Fig. 18 Comparison between target and simulated response spectra of underground motions. **a** Location A', **b** Location B', **c** Location C'

effect. Additionally, as shown in Fig. 18, the simulated underground response spectrum is consistent with the target response spectrum, which further demonstrates the reliability and efficiency of the theoretical method and visual program for simulating the earthquake underground motions.

6 Sensitivity analysis for structural responses under multi-support earthquake underground and ground motions

In this section, the finite element models of a two-span bridge and corresponding soil-bridge system are exemplified for further discussion. Firstly, the multi-support earthquake ground motions are adopted for the numerical analysis of bridge and the seismic response is obtained. Then, the multi-support earthquake underground motions are generated by the visual program as mentioned above. It should be pointed out that the Clough–Penzien model for soft soil site is employed in the program and the parameters of the PSD model, i.e., S_0 , ω_g , ξ_g , ω_f , and ξ_f , are set to 62.38, 6.86, 1.06, 0.84 and 1.42, respectively. Moreover, the Hao Hong coherence model is employed in the generation of underground earthquake acceleration history. Under the earthquake underground excitation, the numerical analyses for seismic responses of bridge and soil-bridge system are performed. Corresponding material parameters are given in Figs. 19 and 20. For the bridge, elastic modulus E_1 , material density ρ_1 , inertial moment I_1 and cross sectional area A_1 are assigned to 2.06×10^{11} Pa, 7800 kg/m^3 , 0.83 m^4 and 1 m^2 , respectively. The elastic modulus (E_2) and density (ρ_2) of soft soil site are assigned 5×10^8 Pa and 2500 kg/m^3 , respectively. Moreover, the local in-plane stiffness matrix for beam elements, K^c , is defined as

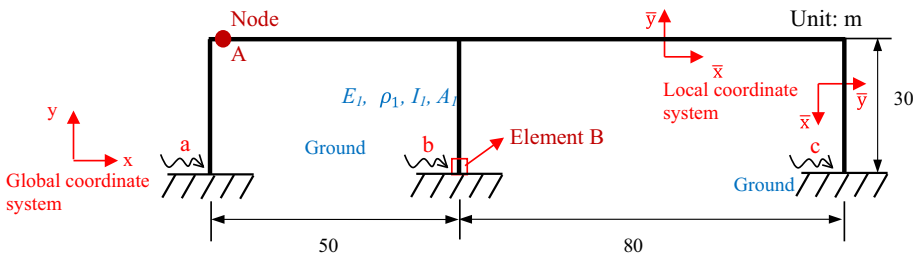


Fig. 19 Finite element model of bridge. Elastic modulus E_1 , material density ρ_1 , inertial moment I_1 and cross sectional area A_1 are assigned to 2.06×10^{11} Pa, 7800 kg/m^3 , 0.83 m^4 and 1 m^2 , respectively

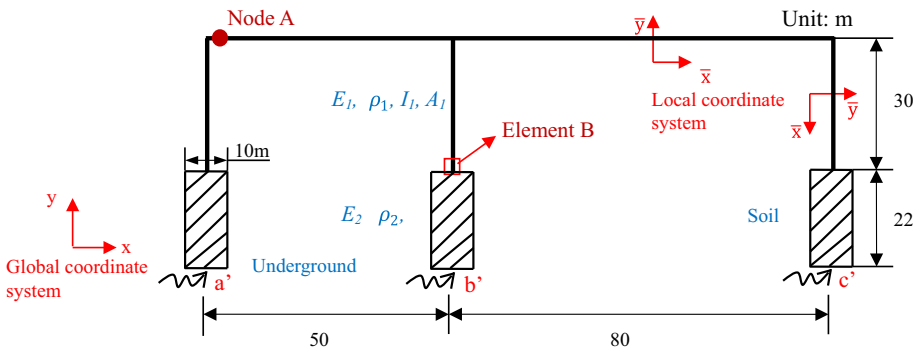


Fig. 20 Finite element model of soil-bridge system. Soil elastic modulus E_2 and density ρ_2 are assigned 5×10^8 Pa and 2500 kg/m^3 , respectively. Material parameters of bridge structure are given in Fig. 19

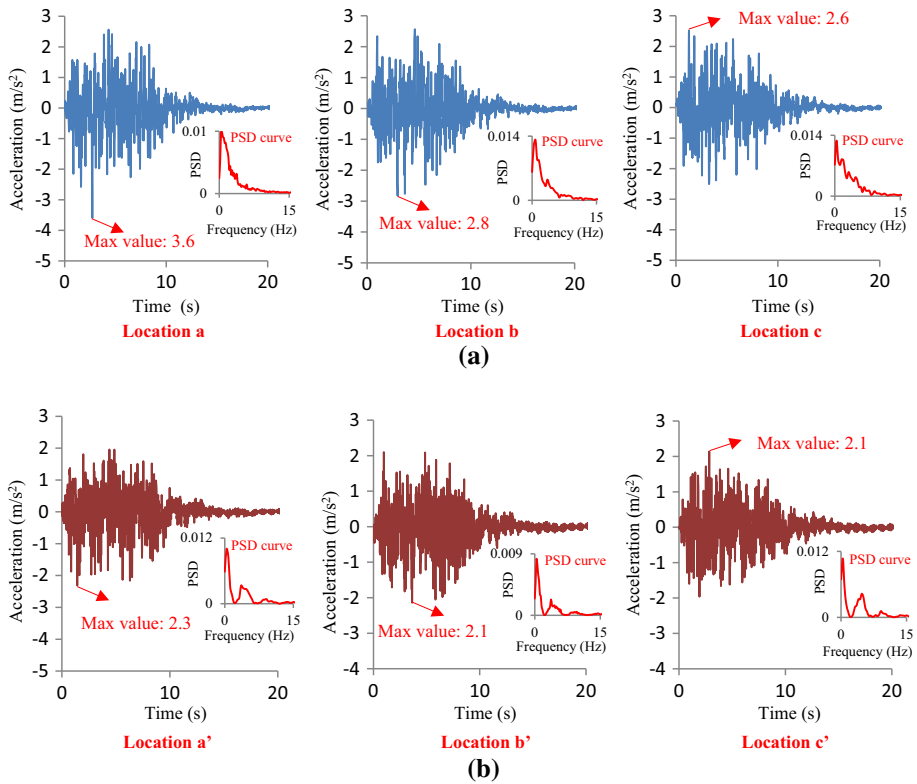


Fig. 21 Ground and underground acceleration histories at the pier positions. **a** Ground acceleration for bridge, **b** Underground acceleration for soil-bridge system

$$K^c = \begin{bmatrix} E_1 A_1 / L & 0 & 0 & 0 & 0 \\ & 12 E_1 I_1 / L^3 & 6 E_1 I_1 / L^2 & -12 E_1 I_1 / L^3 & 6 E_1 I_1 / L^2 \\ & & E_1 I_1 / L & -6 E_1 I_1 / L^2 & E_1 I_1 / L \\ & & & 0 & 0 \\ sym & & & 12 E_1 I_1 / L^3 & -6 E_1 I_1 / L^2 \\ & & & & E_1 I_1 / L \end{bmatrix}$$

where L represents the element length and other involved parameters are given in Fig. 19 (Fig. 21).

As shown in Table 2, the natural frequencies of the bridge and soil-bridge system are calculated and compared with each other. It can be seen from Figs. 22 and 23 that the energy distribution of earthquake motions, no matter ground or underground, is mainly concentrated in the low frequency region ranging from 1 to 5 Hz. Therefore, the high-order natural frequencies have little influence on the dynamic response of structure. In Table 2, the frequencies higher than 15 Hz are ignored and represented by dashed lines (-). The natural frequencies of bridge are much higher than those of soil-bridge system.

As illustrated in Fig. 21, the amplitude of the earthquake underground motion is smaller than that of the earthquake ground motion. However, according to Fig. 24, the absolute displacement of the soil-bridge system is larger than that of the bridge. It is

Table 2 Comparison between natural frequencies of bridge and soil-bridge system

	1	2	3	4	5	6	7	8	9	10
Mode										
Natural frequency (Hz)										
Bridge	1.144	1.447	3.273	4.184	7.574	8.796	9.705	10.611	11.539	13.746
Soil-bridge	0.346	0.902	1.166	1.397	1.506	1.761	2.088	2.508	3.713	4.387
Mode	11	12	13	14	15	16	17	18	19	20
Natural frequency (Hz)										
Bridge	14.300	–	–	–	–	–	–	–	–	–
Soil-bridge	4.495	4.687	5.159	6.947	7.023	7.170	7.184	7.853	8.086	9.334
Mode	21	22	23	24	25	26	27	28	29	30
Natural frequency (Hz)										
Bridge	–	–	–	–	–	–	–	–	–	–
Soil-bridge	10.609	10.761	11.152	12.167	12.925	14.397	14.799	–	–	–

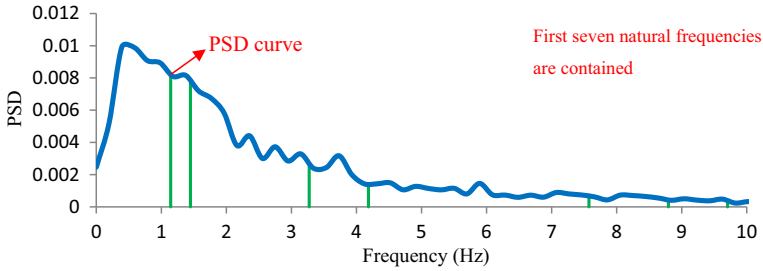


Fig. 22 Distribution of bridge frequencies and ground motion PSD. Vertical lines represent the natural frequencies of bridge

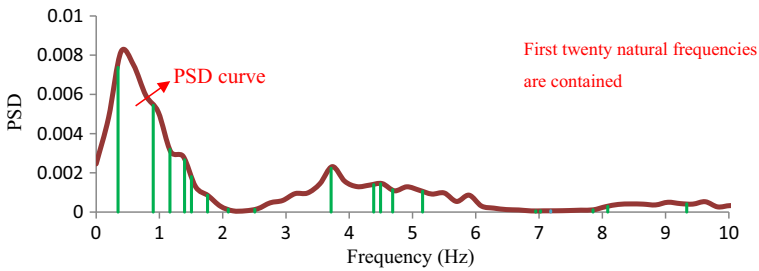


Fig. 23 Distribution of soil-bridge system frequencies and underground motion PSD. Vertical lines represent the natural frequencies of soil-bridge system

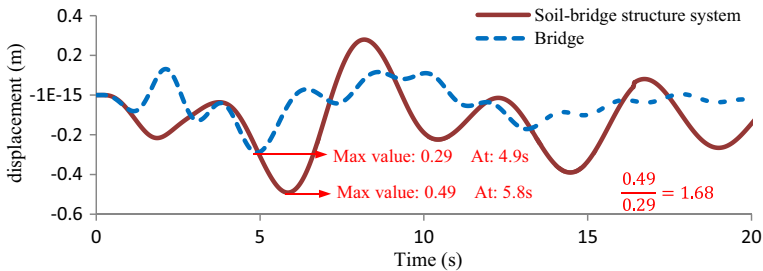


Fig. 24 Comparison between the displacement histories of node A

known that both the amplitude and the frequency have a significant influence on the dynamic response of structure. The natural frequencies of the bridge shown in Fig. 22 are quite high and poorly match the PSD curve. Conversely, the natural frequencies of the soil-bridge system are much lower and match the PSD curve very well. Under the influence of resonance effect, the peak displacement history of the soil-bridge system is larger than that of the bridge, although the amplitude of the underground acceleration history is smaller than that of the ground acceleration history. Furthermore, as illustrated in Fig. 25, the shear force amplitude of the bridge is smaller than that of soil-bridge system for the same reason. It is known that the difference in the support motions increases the structural internal forces, and in this example the structural shear force is

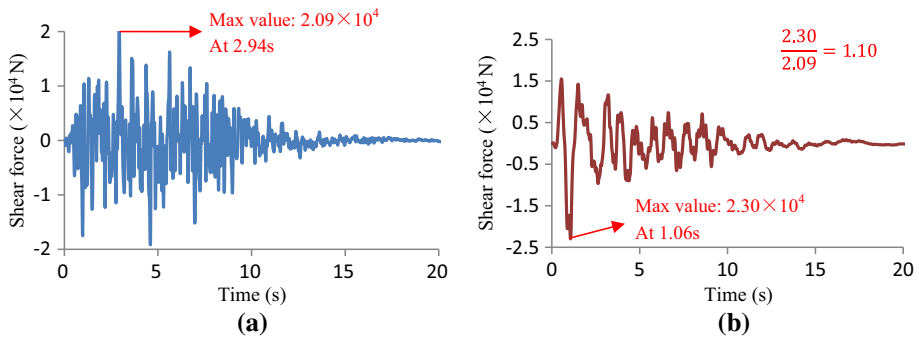


Fig. 25 Comparison between the shear force histories of element B. **a** Bridge, **b** soil-bridge system

even higher under the underground excitation, which may have a significant influence in engineering practice.

7 Concluding remarks

For the seismic analysis of long-span structural system with underground structure, it is important and necessary to use multi-support earthquake underground motions as input excitations. An attempt has been made to simulate multi-support earthquake underground motions and the main works are summarized as follows:

1. An effective approach to simulate the multi-support earthquake underground motions is proposed and the key factor of this approach (i.e. underground cross-correlation function) is deduced. In this paper, the underground PSD and response spectrum are firstly derived and the cross-correlation function between the underground motions at positions with different horizontal and vertical coordinates is further presented. Moreover, the physical meanings of the parameters in the theoretical deduction and mathematical models are clarified.
2. A visual program to simulate the multi-support earthquake underground motions is developed and verified, and the sensitivity analysis for the seismic response under multi-support earthquake ground and underground motions is performed. Results indicate that the simulation of multi-support earthquake underground motions is of great significance for both theoretical study and engineering application.
3. In this paper, it is noted that the underground model such as underground PSD, response spectrum and coherence model are derived using the transfer function of the vertically propagating shear waves. Therefore, the important participation of more complex waves should be further investigated.

Acknowledgements This work was supported by the National Natural Science Foundation of China (Grant Nos. 51408409 and 51579173) and the Tianjin Research Program of Application Foundation and Advanced Technology (Grant No. 15JCQNJC07400).

References

- Abrahamson NA, Schneider JF, Stepp JC (1991) Empirical spatial coherency functions for application to soil-structure interaction analyses. *Earthq Spectra* 7(1):1–27
- Alexander NA (2008) Multi-support excitation of single span bridges, using real seismic ground motion recorded at the SMART-1 array. *Comput Struct* 86(1–2):88–103
- Atkinson KE (1978) An introduction to numerical analysis. Wiley, New York
- Berrah M, Kausel E (1992) Response spectrum analysis of structures subjected to spatially varying motion. *Earthq Eng Struct Dyn* 21(6):461–470
- Bi K, Hao H (2011) Influence of irregular topography and random soil properties on coherency loss of spatial seismic ground motions. *Earthq Eng Struct Dyn* 40(9):1045–1061
- Bi K, Hao H (2012) Modelling and simulation of spatially varying earthquake ground motions at sites with varying conditions. *Probab Eng Mech* 29:92–104
- Chopra AK (2001) Dynamics of structures: theory and applications to earthquake engineering, 2nd edn. Prentice Hall, Englewood Cliffs
- Clough RW, Penzien J (1993) Dynamics of structures, 2nd edn. McGraw-Hill Inc, New York
- Der Kiureghian A (1996) A coherency model for spatially varying ground motions. *Earthq Eng Struct Dyn* 25(1):99–111
- Guo W, Yu ZW, Liu GH, Guo Z (2013) Possible existing seismic analysis errors of long span structures and bridges while utilizing multi-point earthquake calculation models. *Bull Earthq Eng* 11(5):1683–1710
- Hao H (1989) Effects of spatial variation of ground motion on large multiply-supported structures. In: EERC Rep No 89-06, Earthquake Engineering Research Center, University of California, Berkeley
- Hao H, Oliveira CS, Penzien J (1989) Multiple-station ground motion processing and simulation based on smart-1 array data. *Nucl Eng Des* 111(3):293–310
- Kiureghian AD, Neumhoffer A (1992) Response spectrum method for multi-support seismic excitations. *Earthq Eng Struct Dyn* 21(8):713–740
- Konakli K, Der Kiureghian A (2012) Simulation of spatially varying ground motions including incoherence, wave-passage and differential site-response effects. *Earthq Eng Struct Dyn* 41(3):495–513
- Liu GH, Li HN, Tian L (2009) Response analysis of JIUJIANG Yangtze River highway bridge under spatially variable earthquake ground motions. *J Vib Shock* 28(9):204–209 (in Chinese)
- Liu GH, Lu XZ, Guo W (2012) Multi-point seismic motions based on focal mechanism and considering local site multi-layer soil effect: theory and program implementation. *Chin J Comput Mech* 29(4):582–588 (in Chinese)
- Lou L, Zerva A (2005) Effects of spatially variable ground motions on the seismic response of a skewed, multi-span, RC highway bridge. *Soil Dyn Earthq Eng* 25(7):729–740
- Maharaj KK (1978) Stochastic characterization of earthquakes through their response spectrum. *Earthq Eng Struct Dyn* 6(5):497–509
- MOHURD (2011) Code for seismic design of urban bridge (CJJ 166-2011). Ministry of Housing and Urban-Rural Development of the People's Republic of China, Beijing (in Chinese)
- Schnabel PB, Lysmer J, Seed HB (1972) SHAKE: a computer program for earthquake response analysis of horizontally layered sites. Report No. UCB/EERC-72/12, University of California, Berkeley
- Sextos AG, Kyriazis DP, Andreas JK (2003) Inelastic dynamic analysis of RC bridges accounting for spatial variability of ground motion, site effects and soil-structure interaction phenomena. Part 1: methodology and analytical tools. *Earthq Eng Struct Dyn* 32(4):607–627
- SHAKE2000 Consulting Group (2000) SHAKE2000 User's manual, Berkeley
- Shrestha B, Hao H, Bi K (2014) Effectiveness of using rubber bumper and restrainer on mitigating pounding and unseating damage of bridge structures subjected to spatially varying ground motions. *Eng Struct* 79:195–210
- Soize C (2006) Non-Gaussian positive-definite matrix-valued random fields for elliptic stochastic partial differential operators. *Comput Method Appl M* 195(1):26–64
- Su L, Shi JT (2013) Displacement-based earthquake loss assessment methodology for RC frames infilled with masonry panels. *Eng Struct* 48:430–441
- Su L, Dong SL, Kato S (2006) A new average response spectrum method for linear response analysis of structures to spatial earthquake ground motions. *Eng Struct* 28(13):1835–1842
- Ta Q-A, Clouteau D, Cottareau R (2010) Modeling of random anisotropic elastic media and impact on wave propagation. *Eur J Comput Mech* 19(1–3):241–253
- Tian L, Li HN (2012) Seismic response of power transmission tower-line system under multi-component multi-support excitations. *J Earthq Tsunami* 6(4):1250025
- Tian YJ, Yang QS (2009) On time-step in structural seismic response analysis under ground displacement/acceleration. *Earthq Eng Eng Vib* 8(3):341–347

- Tian L, Ma RS, Li HN, Zhang P (2014) Seismic response of straight line type and broken line type transmission lines subjected to non-uniform seismic excitations. *Adv Steel Constr* 10(1):85–98
- Xu ZD (2010) Review for dynamic researches in civil engineering in recent years. *Sci China Technol Sci* 53(5):1450–1452
- Ye JH, Zhang ZQ, Chu Y (2011) Strength behavior and collapse of spatial-reticulated structures under multi-support excitation. *Sci China Ser E* 54(6):1624–1638
- Yu RF, Zhou XY (2008) Response spectrum method analysis for non-classically damped linear system with multiple-support excitations. *Bull Earthq Eng* 6(2):261–284
- Zentner I, Poirion F (2012) Enrichment of seismic ground motion databases using Karhunen–Loève expansion. *Earthq Eng Struct Dyn* 41(14):1945–1957
- Zerva A (1990) Response of multi-span beams to spatially incoherent seismic ground motions. *Earthq Eng Struct Dyn* 19(6):819–832
- Zerva A (2002) Spatial variation of seismic ground motions: an overview. *Appl Mech Rev* 55(3):271–297
- Zerva A (2009) Spatial variation of seismic ground motions: modeling and engineering applications (Advances in engineering series). CRC Press, Boca Raton
- Zhang N, Xia H, Roeck GD (2010) Dynamic analysis of a train-bridge system under multi-support seismic excitations. *J Mech Sci Technol* 24(11):2181–2188